Optimization of Synthetic Aperture Image Quality

Moshavegh, Ramin; Jensen, Jonas; Villagómez Hoyos, Carlos Armando; Stuart, Matthias Bo; Hemmsen, Martin Christian; Jensen, Jørgen Arendt

Published in:
Proceedings of SPIE

Link to article, DOI:
10.1117/12.2216506

Publication date:
2016

Document Version
Peer reviewed version

Optimization of Synthetic Aperture Image Quality

Ramin Moshavegh[a], Jonas Jensen[a], Carlos A. Villagomez-Hoyos[a], Matthias B. Stuart[a], Martin Christian Hemmsen[a], and Jørgen Arendt Jensen[a]

[a]Center for Fast Ultrasound Imaging, Department of Electrical Engineering, Technical University of Denmark, DK-2800 Lyngby, Denmark

ABSTRACT

Synthetic Aperture (SA) imaging produces high-quality images and velocity estimates of both slow and fast flow at high frame rates. However, grating lobe artifacts can appear both in transmission and reception. These affect the image quality and the frame rate. Therefore optimization of parameters effecting the image quality of SA is of great importance, and this paper proposes an advanced procedure for optimizing the parameters essential for acquiring an optimal image quality, while generating high resolution SA images. Optimization of the image quality is mainly performed based on measures such as F-number, number of emissions and the aperture size. They are considered to be the most contributing acquisition factors in the quality of the high resolution images in SA. Therefore, the performance of image quality is quantified in terms of full-width at half maximum (FWHM) and the cystic resolution (CTR). The results of the study showed that SA imaging with only 32 emissions and maximum sweep angle of 22 degrees yields a very good image quality compared with using 256 emissions and the full aperture size. Therefore the number of emissions and the maximum sweep angle in the SA can be optimized to reach a reasonably good performance, and to increase the frame rate by lowering the required number of emissions. All the measurements are performed using the experimental SARUS scanner connected to a $\lambda/2$-pitch transducer. A wire phantom and a tissue mimicking phantom containing anechoic cysts are scanned using the optimized parameters for the transducer. Measurements coincide with simulations.

Keywords: Synthetic aperture, FWHM, cystic resolution, grating lobes, Multi objective optimization, Pareto optimal, ultrasound imaging

1. INTRODUCTION

Synthetic aperture imaging (SA) addresses the problems with low frame rate in conventional ultrasound imaging, where one line at a time is beamformed for generating the final ultrasound image. In SA emissions with large areas of sonification can be used and a complete resolution image can be beamformed for each emission. By combining all the low resolution images the final high resolution image is generated.[1]

Number of emissions and aperture size are two parameters strongly effecting the quality of the high resolution images in SA imaging. Different scenarios also require different values of these parameters. For the case of B-mode SA imaging, the number of emissions can be kept quite high, whereas when flow estimates are needed, less emissions and consequently high frame rates are interesting.[2–5]

This paper presents a pilot study of image quality optimization for SA based on the performance measures of full-width at half maximum (FWHM) and the cystic resolution (CTR). All the possible imaging setups for different number of emissions and aperture sizes are considered for a $\lambda/2$-pitch linear transducer. Six point scatterers located underneath the transducer are simulated using the Field II program.[6–8] For each possible combination of number of emissions N and the aperture size α_{max}, the CTR and FWHM are computed for all scatterers and the values recorded. Third, two independent plots featuring the CTR and FWHM as a function of α_{max} and N are generated. The information of the two plots are then merged and scatter-plotted as all possible setups. A Pareto optimization procedure[10,11] is then applied to the scatterer plot to identify the optimal setups in terms of having low CTR and also relatively small FWHM. The remainder of this paper is organized as follows. Section 2 introduces the proposed algorithm. Section 3 presents the results of the proposed method and discusses the findings. Finally section 4 is the conclusion and the perspectives.

Further author information: Ramin Moshavegh, E-mail: ramosh@elektro.dtu.dk

TABLE 1: Parameters used for simulation.

Parameters	λ/2-pitch transducer
Number of elements	192
Transducer center frequency f_0	4.1 MHz
Wavelength λ	0.376 mm
Element pitch	0.2 mm (0.56λ)
Element height	6 mm
Elevation focus	38 mm
Cycles in emitted pulse	1
Transmit apodization	Hamming
Receive apodization	Hamming
Receive F-number	1
Emission steering angles	-30°:0.25°:+30°

2. MATERIALS AND METHODS

This section first presents the quality metrics used in the study for optimization of SA image quality, and then details the optimization procedure.

2.1 Imaging performance measures

Two of the main quality metrics used in the literature for evaluating the performance of the ultrasound imaging quality are cystic resolution (CTR) and full-width in half maximum (FWHM). This paper uses these two features and all the optimizations are performed based on the rate of the changes in these features while moving between setups by changing the sweep angle (corresponding to the aperture size) α_{max} and the number of emissions N.

The CTR measures the contrast resolution and determines the ability of the imaging system to differentiate between an anechoic region bracketed within a uniform scattering medium. Ranganathan and Walker[9] quantified CTR as the ratio between the energy outside of a circular area surrounding the point spread function (PSF) with radius of R to the total energy of the PSF. Therefore it gives a measure of clutter energy outside the main lobe of the PSF.

The FWHM on the other hand measures the detail resolution. It is a measure of the width of the main lobe of the PSF. The FWHM is usually measured both axially and laterally and those are both influenced by the bandwidth of the imaging system. The lateral FWHM is also dependent on the pulse wavelength, size of the aperture (F number), and the maximum steering angle of the emissions.

2.2 Method of optimization

This section describes the method of multi-objective optimization used in this study for optimizing the SA image quality based on the theory of Pareto optimality.[10] In many circumstances, solutions in the presence of the conflicting objectives are needed. In such cases, solutions are chosen such that sensible trade-offs exist among different objectives. Pareto optimization is used for finding these solutions. In this multi-objective optimality theory, many solutions are found that satisfy the Pareto optimality criterion.[11] This criterion considers a solution to be optimum only if there are no other solutions better than that with respect to all the objectives. A solution $\mathbf{x}' = \{x_1, x_2\}$ is a Pareto optimal solution if there exists no other solutions like $\mathbf{x}$ for which $\mathbf{P}$ dominates $\mathbf{P}'$. Notice, F is the objective function. A point $\mathbf{P}$ is dominating another point $\mathbf{P}'$ (mathematically given by $\mathbf{P} \preceq \mathbf{P}'$), when $\mathbf{P}$ is no worse than $\mathbf{P}'$ in all objectives, and $\mathbf{P}$ is strictly better than $\mathbf{P}'$ in at least one objective. Therefore a pareto optimal solution is given by

$$\mathcal{P}^* := \left\{ \mathbf{x}' \mid \nexists\, \mathbf{x} :\ \mathbf{P} \preceq \mathbf{P}' \right\}. \tag{1}$$

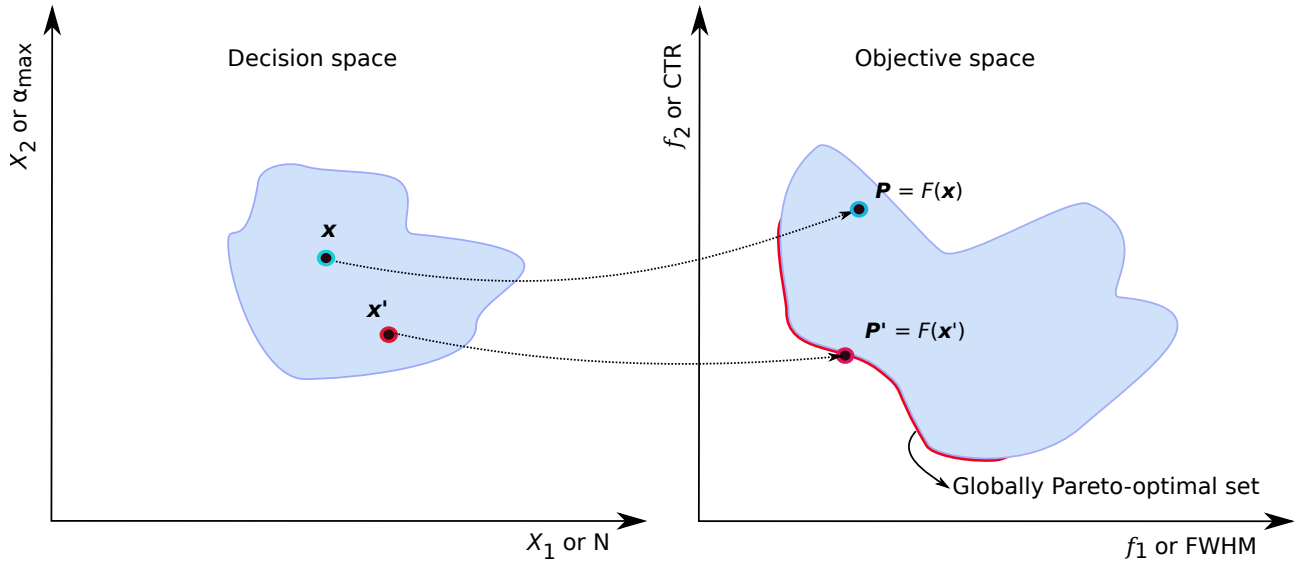

Figure 1: Illustration of how the Pareto optimization is performed.The decision space contains independent variables whereas the objective space contains the dependent variables. The set of all Pareto optimal solutions or Pareto front is shown with the red curve.

The set of all optimal solutions is called Pareto front or curve or surface (see red curve in Fig. 1). The shape of the Pareto front manifests the nature of trade-off between different objectives. In this study the pareto optimization is applied to a two-objective problem, in which two conflicting parameters are required to be optimized. The Pareto front is particularly interesting because it contains the solutions where improvement in one variable is not possible without jeopardizing the other. Hence, in this study only the Pareto optimal solutions are considered while optimizing the SA image quality. Section 2.4 describes how the Pareto optimization is applied in the study.

2.3 Simulations

A $\lambda/2$-pitch transducer pitch transducer was modelled and six different point scatterers were simulated axially located underneath the transducer and positioned 10 mm apart from each other. Simulations were performed using the Field II program[6–8] (see Table 1 for details of the parameters used). A Hamming apodization on the active transmit aperture was used to reduce the edge waves. In SA emissions were set to steer from -30° to +30° with 0.25° separation between emissions. Received signals from all elements were stored for each emission and beamformation were performed using the BFT3 toolbox.[12] The beamformed low-resolution images were subsequently combined to high-resolution images. Several high-resolution images were generated by varying maximum beam steered angle (α_{max}) and the number of emissions (N). The image quality of the high-resolution images were then evaluated by computing both CTR and the lateral FWHM for simulated point scatterers. For each simulated scatterer two plots were generated. First one quantifying the CTR as a function of α_{max} and N, and the second quantifying the FWHM as a function of α_{max} and N. These images are used in the Section 2.4 to construct the objective space plots to optimize the two dependent variables of maximum beam steered angle (α_{max}) and the number of emissions (N)

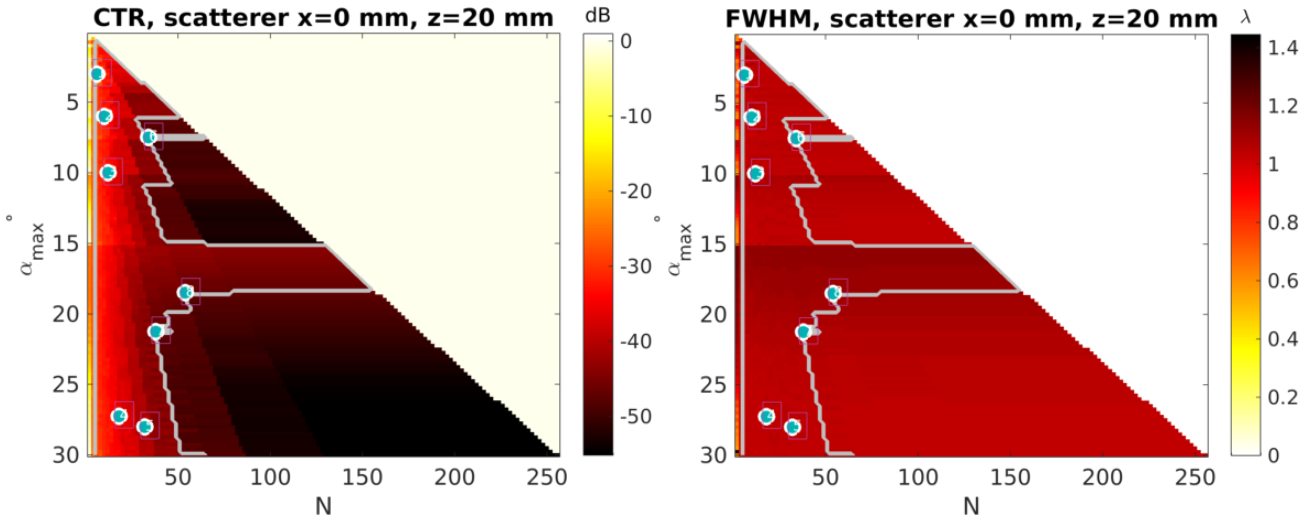

(a) CTR computed as a function of α_{max} and N for scatterer at 20 mm.

(b) FWHM as a function of α_{max} and N for scatterer at 20 mm.

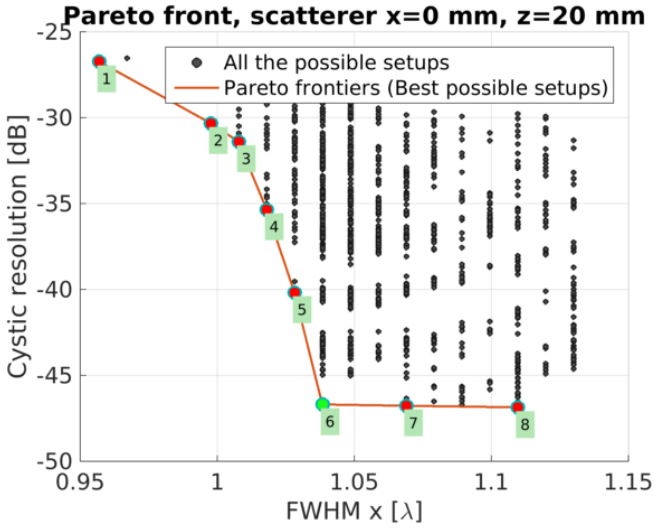

(c) Pareto made by merging the CTR and FWHM for scatterer at 20 mm.

Figure 2: Optimization procedure demonstrated for the scatterer at 20 mm from the surface of the transducer.

2.4 Optimization of the setup

This section discusses the optimization performed to find the optimal setup for the SA image quality in terms of α_{max} and N. The information regarding the CTR and FWHM in two plots generated for each scatterer in Section 2.3 were merged and and a Pareto plot (scatterer plot of all possible setups) was generated for each scatterer. On the Pareto plot, the Pareto front or all the optimal setups in terms of CTR and FWHM were computed, whereby any improvement with respect to CTR comes at the expense of FWHM and vice-versa. The Pareto front in a sense characterise the setups in which the FWHM and CTR values are optimal. The optimal Pareto setups (Pareto fronts) for all scatterers were then combined in one plot and the center of the gravity for all the optimal setups was considered to be the optimal setup for the SA imaging.

2.5 Phantom measurements

Phantom measurements were made using the SARUS experimental ultrasound scanner[13] driving a 192-element 4.1 MHz $\lambda/2$-pitch linear transducer (8L2, BK Ultrasound). A synthetic aperture B-mode imaging sequence using the virtual sources behind transducer was used to perform the imaging. Parameters used in the imaging sequence are depicted in the Table 1. First, A geometry wire phantom including three wires was scanned. A multi purpose, multi-yissue phantom containing three anechoic cysts located at 17 mm, 48 mm, and 75 mm (Model 040GSE, CIRS inc., Virgina, USA) with acoustic attenuation of 0.5 dB/(cm.MHz) was also scanned.

3. RESULTS AND DISCUSSION

The results of CTR, FWHM and Pareto optimizations for one of the scatterers located 20 mm underneath the transducer is shown in the Fig. 2. Fig. 3 also shows all the optimal setups corresponding to the Pareto fronts of all 6 different scatterers combined in one plot. The yellow diamond ($\alpha_{max} = 22^\circ$ and $N = 32$) is the center of the gravity of all points and the optimal setup for the SA. This optimal setup requires 32 emissions and 22° maximum sweeping angle. The other observation was made in the Fig. 4, in which a point scatterer at 20 mm was simulated and the high resolution images of the scatterer were reconstructed using three different number of emissions. The PSFs for high-resolution images made of 32 and 256 emissions are quite identical. The same observation was also made on the measured wire phantom using varying number of emissions. Fig. 5 shows the measured PSFs belonging to two point scatterers located at 32.5 mm and 57.5 mm. Each PSF was reconstructed with 4, 32 and 256 emissions, where the 32 emissions is the optimized sequence. The point PSFs reconstructed with 32 emissions are quite similar to the one reconstructed with 256 emissions. Fig. 6 shows two phantoms measured with $N = 4$, the optimized sequence ($\alpha_{max} = 22^\circ$ and $N = 32$), and also $N = 256$. This set of measurements also indicated that the quality of the image does not improve by increasing the emissions to more than 32. A set of this indicates that for achieving a reasonably good image quality the number of emissions does not have to be increased to more than the optimal value computed for the SA.

4. CONCLUSION

This paper presented a hierarchical method for characterising the optimal setup in SA imaging. The results showed that with only $\alpha_{max} = 22^\circ$ and $N = 32$, the image quality is reasonably good and comparable with high number of emissions. Improvements in frame rate is also achievable by using less number of emissions. This can more highlighted when high frame rate is needed for velocity estimation, and when the standard deviation of the velocity estimates are related to the frame rate. The optimized sequence also enables fast acuisition of SA images without degrading the quality. This is rather crucial when the real-time automatic segmentation of vessels are performed.

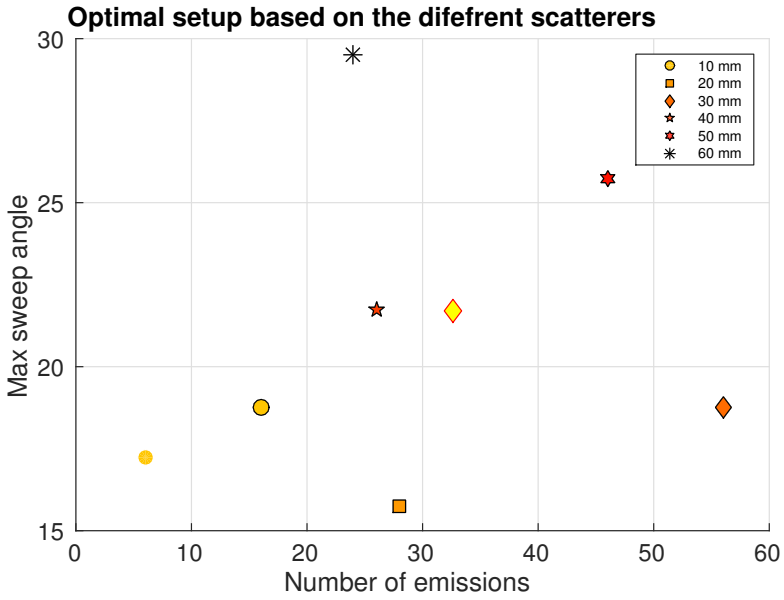

Figure 3: Combination of all the optimal setups (Pareto fronts) belonging to all scatterers in one plot.

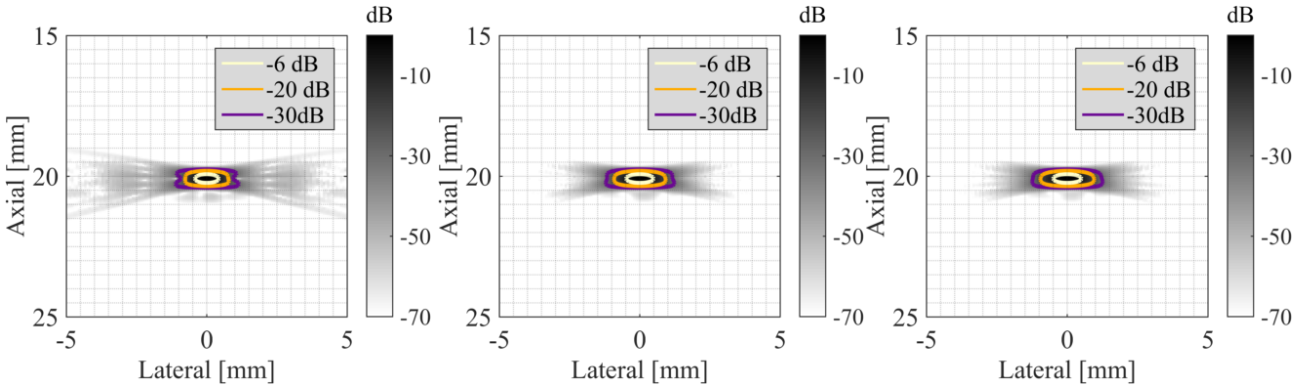

(a) Reconstructed from 4 emissions. (b) Reconstructed from 32 emissions. (c) Reconstructed from 256 emissions.

Figure 4: Comparison of the high-resolution image of the scatterer at 20mm reconstructed from low, optimal and high number of emissions.

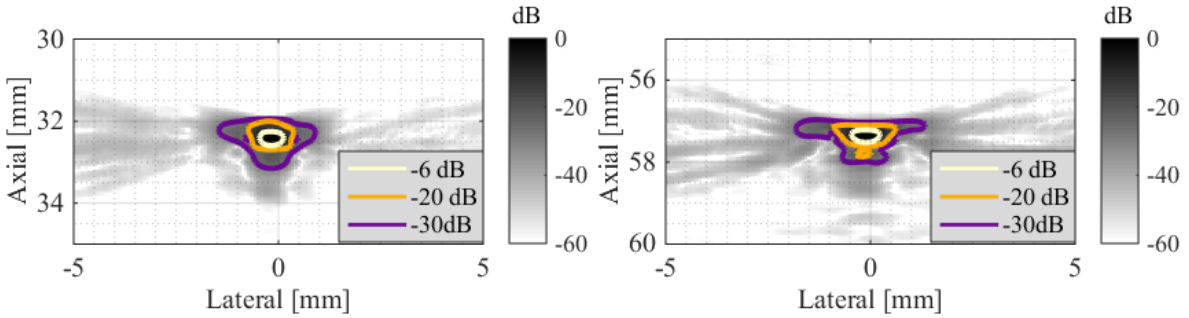

(a) Reconstructed from 4 emissions.

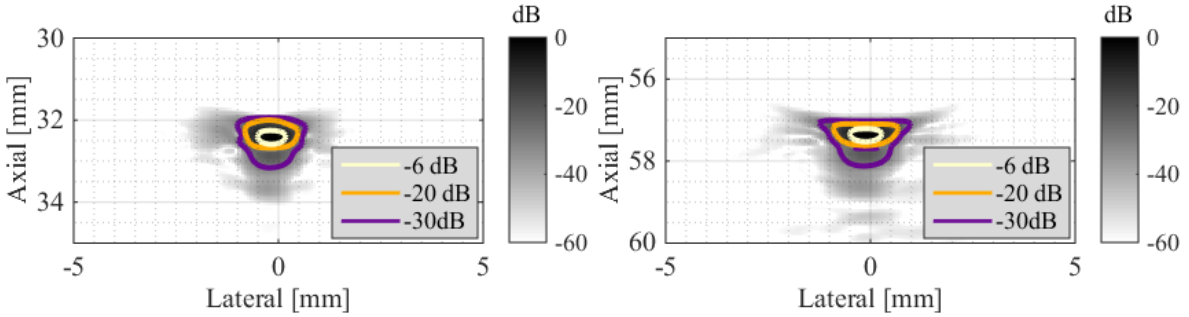

(b) Reconstructed from 32 emissions.

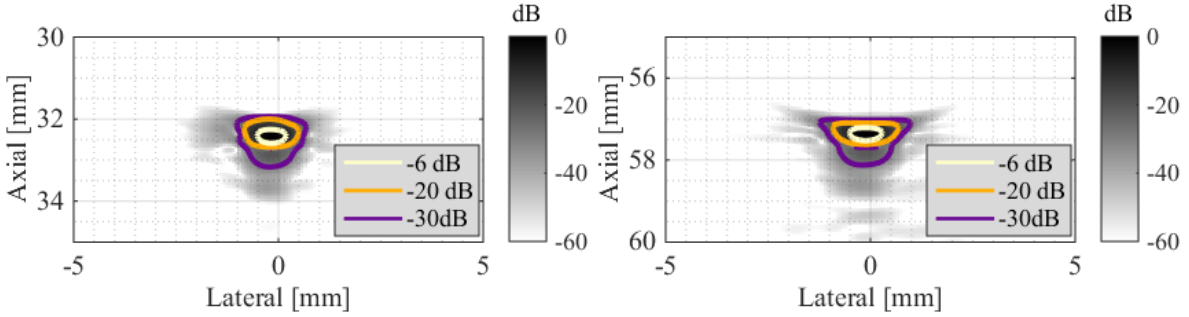

(c) Reconstructed from 256 emissions.

Figure 5: Comparison of the high-resolution image of the scatterer at 20mm reconstructed from low, optimal and high number of emissions.

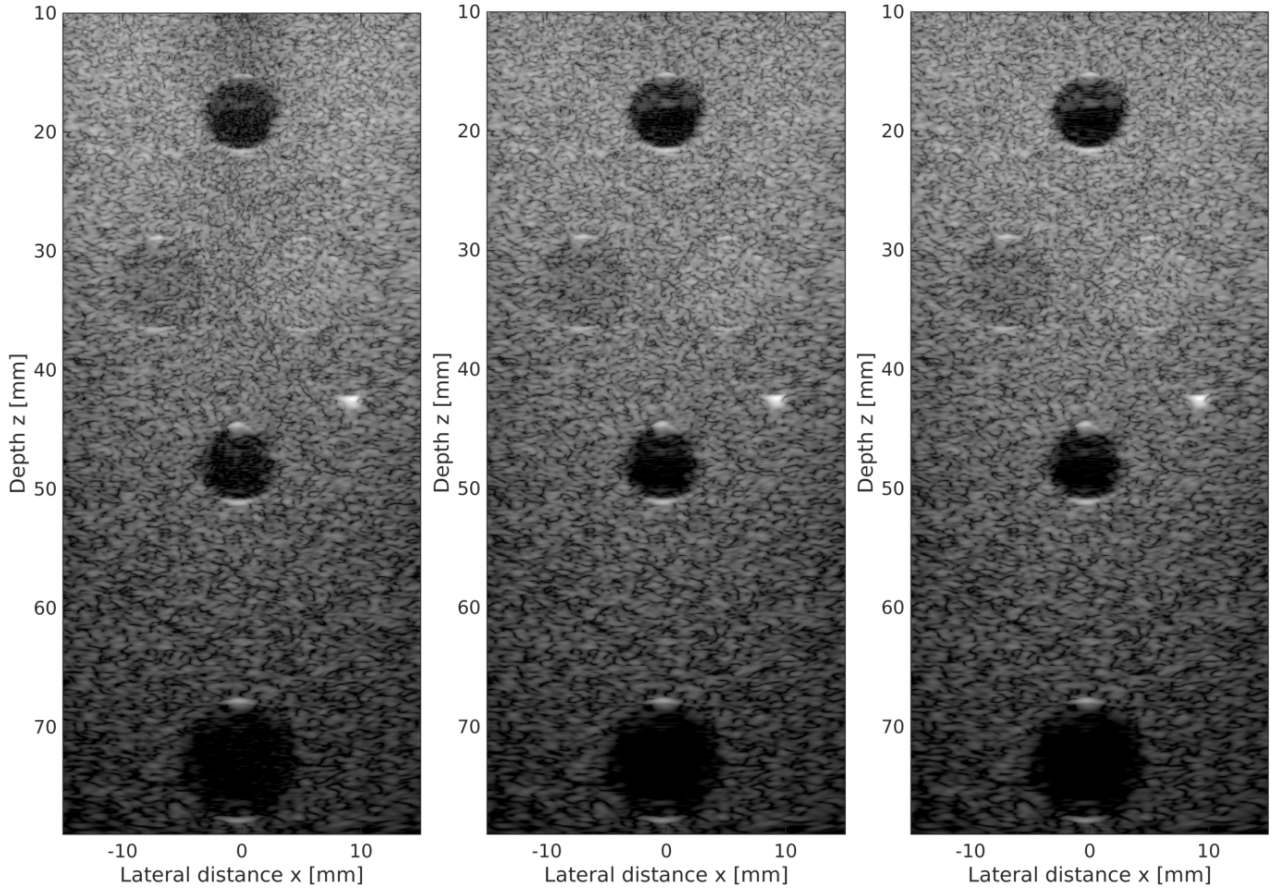

(a) Reconstructed from 8 emissions. (b) Reconstructed from 32 emissions. (c) Reconstructed from 256 emissions.
Figure 6: Measured cyst phantom and reconstructed from low, optimal and high number of emissions. All three images are shown in 60 dB dynamic range.

REFERENCES

[1] Jensen, J. A., Nikolov, S., Gammelmark, K. L., and Pedersen, M. H., "Synthetic aperture ultrasound imaging," *Ultrasonics* **44**, e5–e15 (2006).

[2] Nikolov, S. I., Gammelmark, K., and Jensen, J. A., "Recursive ultrasound imaging," in [*Proc. IEEE Ultrason. Symp.*], **2**, 1621–1625 (1999).

[3] O'Donnell, M. and Thomas, L. J., "Efficient synthetic aperture imaging from a circular aperture with possible application to catheter-based imaging," *IEEE Trans. Ultrason., Ferroelec., Freq. Contr.* **39**, 366–380 (1992).

[4] Karaman, M., Li, P. C., and O'Donnell, M., "Synthetic aperture imaging for small scale systems," *IEEE Trans. Ultrason., Ferroelec., Freq. Contr.* **42**, 429–442 (1995).

[5] Karaman, M. and O'Donnell, M., "Subaperture processing for ultrasonic imaging," *IEEE Trans. Ultrason., Ferroelec., Freq. Contr.* **45**, 126–135 (1998).

[6] Jensen, J. A. and Svendsen, N. B., "Calculation of pressure fields from arbitrarily shaped, apodized, and excited ultrasound transducers," *IEEE Trans. Ultrason., Ferroelec., Freq. Contr.* **39**, 262–267 (1992).

[7] Jensen, J. A., "Field: A program for simulating ultrasound systems," *Med. Biol. Eng. Comp.* **10th Nordic-Baltic Conference on Biomedical Imaging, Vol. 4, Supplement 1, Part 1**, 351–353 (1996).

[8] Jensen, J. A., "A multi-threaded version of Field II," in [*Proc. IEEE Ultrason. Symp.*], 2229–2232, IEEE (2014).

[9] Coello, C. A. C., Lamont, G. B., and Veldhuizen, D. A. V., [*Evolutionary Algorithms for Solving Multi-Objective Problems*], Springer (2007).

[10] Deb, K., "Multi-objective optimization," in [*Search methodologies*], Springer (2005).

[11] Ranganathan, K. and Walker, W. F., "Cystic resolution: A performance metric for ultrasound imaging systems," *IEEE Trans. Ultrason., Ferroelec., Freq. Contr.* **54**(4), 782–792 (2007).

[12] Hansen, J. M., Hemmsen, M. C., and Jensen, J. A., "An object-oriented multi-threaded software beamformation toolbox," in [*Proc. SPIE Med. Imag.*], **7968**, 79680Y 1–9 (March 2011).

[13] Jensen, J. A., Holten-Lund, H., Nilsson, R. T., Hansen, M., Larsen, U. D., Domsten, R. P., Tomov, B. G., Stuart, M. B., Nikolov, S. I., Pihl, M. J., Du, Y., Rasmussen, J. H., and Rasmussen, M. F., "SARUS: A synthetic aperture real-time ultrasound system," *IEEE Trans. Ultrason., Ferroelec., Freq. Contr.* **60**(9), 1838–1852 (2013).